Pure Bending Flutter of a Swept Wing in a High-Density, Low-Speed Flow

JOHN DUGUNDJI* AND NANCY GHAREEB†
Massachusetts Institute of Technology, Cambridge, Mass.

The pure bending flutter of a uniform, high-aspect ratio, swept wing is studied in detail. The velocity-component aerodynamic-strip theory is used with both quasi-steady and unsteady Theodorsen-function representations. Exact solutions of the differential equation are obtained, thereby eliminating problems of modal convergence. Effects of structural damping and below-flutter response are also examined. It is shown that, below certain critical values of mass-density ratio μ, flutter does not occur. Also, at low values of μ, increasing the sweepback of a given wing lowers the flutter speed significantly until a critical angle is reached, beyond which the flutter speed rises sharply to infinity. The mode shapes at flutter change from a standing wave-type at high values of μ to a traveling wave-type at low μ. Quasi-steady theory is generally unconservative in flutter speed when compared with complete unsteady theory. The exact differential-equation solution procedure and general eigenvalue behavior may be of interest in understanding other similar-type instability problems. It is suggested that the solution procedure be extended to include torsion of the wing as well in order to understand better the effect of sweepback on flutter at low mass-density ratios μ.

Nomenclature

A_R, A_I = real and imaginary parts of complex coefficient A in Eq. (10)
B_R, B_I = real and imaginary parts of complex coefficient B in Eq. (10)
$\bar{b}$ = semichord perpendicular to elastic axis
$C(k)$ = Theodorsen function = $F(k) + iG(k)$
c_m = coefficients
D_B = damping in beam
EI = bending rigidity of beam
F, G = real and imaginary parts of $C(k)$ function
g_j = structural damping coefficients of jth mode $\approx 2_x$ (critical damping ratio)
H = parameter = $3.52\, g_h(-B_R)^{1/2}/B$
$h, \bar{h}$ = vertical displacement
i = $(-1)^{1/2}$
K_2 = unsteady parameter = $1 + 2G/k$
k = reduced frequency = $\omega\bar{b}/U\cos\Lambda$
L = lift/ft of length s
ℓ = length of wing along elastic axis
m = mass/ft of length along elastic axis
p = parameter = $\frac{1}{2}(\epsilon B_I/A_I - 1)$
Q = dynamic pressure parameter = $\pi\rho U^2\bar{b}l^3F(\sin 2\Lambda)/EI$
$\tilde{Q}$ = dynamic pressure parameter = $\pi\rho U^2\bar{b}l^3(\sin 2\Lambda)/EI$
R = parameter = $-B_RA_R/B_IA_I$
s = coordinate along elastic axis
t = time
U = velocity of flow
z_m = roots of characteristic equation of Eq. (10)
α, β = real and imaginary parts of complex eigenvalue Ω
Δ = determinant defined by Eq. (14)
ϵ = geometry parameter = $(\bar{b}/2\ell)(\tan\Lambda)/F$
$\tilde{\epsilon}$ = geometry parameter = $(\bar{b}/2\ell)\tan\Lambda$
Λ = sweepback angle
μ = mass-density ratio = $m/\pi\rho\bar{b}^2$
ξ = nondimensional coordinate = s/ℓ
ρ = fluid density
τ = nondimensional time = $t(ml^4/EI)^{1/2}$
Φ = complex function defined by Eq. (15)
ω = frequency of oscillation
ω_h = fundamental wing-bending frequency in vacuum = $3.52(EI/ml^4)^{1/2}$
Ω = complex eigenvalue = $\alpha + i\beta$

Subscripts

R = real
I = imaginary
F = flutter
h = fundamental bending mode

Introduction

IN analytical investigations of bending-torsion flutter of high-aspect ratio, straight wings, the flutter speed increases sharply below a certain mass-density ratio μ.[1, 2] This would prevent flutter from arising on straight-wing hydrofoils, which ordinarily operate at very low mass-density ratios of $\mu \approx 0.20$ or less. However, if the wing is given a small amount of sweepback, the couplings change so as to permit flutter to occur at these very low values of μ.[3–5]

In an attempt to examine this effect of sweepback, the pure bending flutter of a uniform high-aspect ratio, swept wing is investigated in this article. An earlier, partial study of this problem by modal methods was made by Cunningham.[6] To eliminate convergence difficulties caused by an insufficient number of modes being taken, particularly at low values of μ, an exact solution of the partial differential equation will be obtained, rather than a modal solution. This is similar to techniques used in examining panel-flutter behavior at high supersonic speeds.[7, 8] In further work it is hoped to look at the more complete case of bending-torsion flutter by similar methods.

Mathematically, the present problem represents the solution for the eigenvalues of a fourth-order differential equation with complex coefficients. The general nature of the solution and its practical solution may be of interest to people dealing with related equations. The present article is a condensation of a longer report on the subject by the authors.[9]

Presented as Preprint 65-113 at the AIAA 2nd Aerospace Sciences Meeting, New York, N. Y., January 25–27, 1965; revision received February 8, 1965. This work was supported by the U. S. Navy Bureau of Ships, Fundamental Hydrodynamics Research Program S-R009 01 01, administered by David Taylor Model Basin under Contract Nonr-1841(81). The authors wish to acknowledge helpful discussions with H. Ashley and some early assistance by J. Bajoni, J. C. Delmas, and N. Quang Con.

* Associate Professor, Department of Aeronautics and Astronautics. Member AIAA.

† Division of Sponsored Research Staff, Aeroelastic and Structures Research Laboratory.

1. Theory

Consider a uniform, cantilever, high-aspect ratio, swept wing placed in a low-speed flow of velocity U, as shown in Fig. 1. Considering the wing to be infinitely stiff in torsion but quite flexible in bending‡ ($\alpha = 0$, $h \neq 0$), the governing differential equation of motion would be

$$EI(\partial^4 h/\partial s^4) = \bar{L} - m(\partial^2 h/\partial t^2) \tag{1}$$

where $\bar{L}$ represents the lift/ft of length s. Using the velocity-component aerodynamic-strip theory, the lift on this non-twisting wing can be expressed as[10]

$$\bar{L} = -\pi\rho\bar{b}^2[(\partial^2 h/\partial t^2) + (\partial^2 h/\partial s\partial t)U \sin\Lambda] - 2\pi\rho\bar{b}U \cos\Lambda C(k)[(\partial h/\partial t) + (\partial h/\partial s)U \sin\Lambda] \tag{2}$$

where $C(k) = F + iG$ is the Theodorsen function. For some of the development here, quasi-steady lift forces will be assumed,[11, 12] and $C(k)$ will be set equal to a real constant, i.e., $G = 0$. Later in Appendix B, flutter solutions will be obtained with the complete Theodorsen function $F + iG$ for comparison.

Using quasi-steady lift forces, combining Eqs. (1) and (2), and introducing the nondimensional variables ξ and τ defined as

$$\xi = s/\ell \qquad \tau = t/(m\ell^4/EI)^{1/2} \tag{3}$$

will yield the linear partial differential equation

$$\frac{\partial^4 h}{\partial \xi^4} + Q\frac{\partial h}{\partial \xi} + \left(\frac{Q\epsilon}{\mu}\right)^{1/2}\frac{\partial^2 h}{\partial \xi \partial \tau} + \left(\frac{Q}{\mu\epsilon}\right)^{1/2}\frac{\partial h}{\partial \tau} + \frac{\mu + 1}{\mu}\frac{\partial^2 h}{\partial \tau^2} = 0 \tag{4}$$

where Q, μ, and ϵ are nondimensional parameters defined by

$$Q = \pi\rho U^2\bar{b}\ell^3 F(\sin 2\Lambda)/EI \quad \text{dynamic pressure parameter} \tag{5}$$

$$\mu = m/\pi\rho\bar{b}^2 \quad \text{mass-density ratio} \tag{6}$$

$$\epsilon = (\bar{b}/2\ell)(\tan\Lambda)/F \quad \text{geometry parameter} \tag{7}$$

The partial differential equation [Eq. (4)] is to be solved subject to the following boundary conditions:

$$\left.\begin{aligned} &\text{Cantilever End} \\ &\quad \xi = 0 \rightarrow h = 0 \qquad (\partial h/\partial \xi) = 0 \\ &\text{Free End} \\ &\quad \xi = 1 \rightarrow \partial^2 h/\partial \xi^2 = 0 \qquad (\partial^3 h/\partial \xi^3) = 0 \end{aligned}\right\} \tag{8}$$

Solutions of Eq. (4) are assumed in the form

$$h(\xi, \tau) = \bar{h}(\xi)e^{\Omega\tau} \tag{9}$$

Unstable solutions will occur if Ω is real and positive (static instability) or complex with a positive real part (dynamic instability). Setting $\Omega = \alpha + i\beta$ and inserting Eq. (9) into Eq. (4) will yield the total differential equation

$$(d^4\bar{h}/d\xi^4) + (A_R + iA_I)(d\bar{h}/d\xi) + (B_R + iB_I)\bar{h} = 0 \tag{10}$$

where

$$A_R = Q + (Q\epsilon/\mu)^{1/2}\alpha \tag{11a}$$

$$A_I = (Q\epsilon/\mu)^{1/2}\beta \tag{11b}$$

$$B_R = (Q/\mu\epsilon)^{1/2}\alpha + (\alpha^2 - \beta^2)(\mu + 1)/\mu \tag{11c}$$

$$B_I = (Q/\mu\epsilon)^{1/2}\beta + (2\alpha\beta)(\mu + 1)/\mu \tag{11d}$$

The general solution of Eq. (10) is

$$\bar{h} = c_1 e^{z_1\xi} + c_2 e^{z_2\xi} + c_3 e^{z_3\xi} + c_4 e^{z_4\xi} \tag{12}$$

‡ Physically, this occurs for wings of very high-aspect ratio.

where the c_m terms are arbitrary complex constants, and the z_m terms are the four roots of the complex characteristic equation [Eq. (10)]. Inserting $\bar{h}$ into the boundary conditions, Eq. (8) yields the matrix equation

$$\begin{bmatrix} 1 & 1 & 1 & 1 \\ z_1 & z_2 & z_3 & z_4 \\ z_1^2 e^{z_1} & z_2^2 e^{z_2} & z_3^2 e^{z_3} & z_4^2 e^{z_4} \\ z_1^3 e^{z_1} & z_2^3 e^{z_2} & z_3^3 e^{z_3} & z_4^3 e^{z_4} \end{bmatrix}\begin{Bmatrix} c_1 \\ c_2 \\ c_3 \\ c_4 \end{Bmatrix} = \begin{Bmatrix} 0 \\ 0 \\ 0 \\ 0 \end{Bmatrix} \tag{13}$$

For nontrivial solutions of the constants c_m, the roots z_m must make the determinant Δ equal to zero, that is,

$$\Delta = \begin{vmatrix} 1 & 1 & 1 & 1 \\ z_1 & z_2 & z_3 & z_4 \\ z_1^2 e^{z_1} & z_2^2 e^{z_2} & z_3^2 e^{z_3} & z_4^2 e^{z_4} \\ z_1^3 e^{z_1} & z_2^3 e^{z_2} & z_3^3 e^{z_3} & z_4^3 e^{z_4} \end{vmatrix} = 0 \tag{14}$$

At first, the following direct procedures were used to obtain flutter solutions ($\alpha = 0$) of Eqs. (4) and (8). For a given configuration defined by values of μ and ϵ, various values of Q and β were selected, and the four roots z_1, z_2, z_3, and z_4 of the complex characteristic equation [Eq. (10)] were found. Then the complex function Φ was evaluated, where§

$$\Phi = [\Delta/(z_1 - z_2)(z_1 - z_3)(z_1 - z_4)(z_2 - z_3)(z_2 - z_4)(z_3 - z_4)] \tag{15}$$

These values of $\Phi(Q, \beta)$ were plotted in the complex plane. The value Q, β, which made $\Phi(Q, \beta) = 0$ was a flutter solution for the given μ, ϵ configuration. The below-flutter response also was investigated similarly by selecting values of α and β for a given μ, ϵ, Q configuration and finding the values which made $\Phi(\alpha, \beta) = 0$.

At low values of μ, the preceding direct procedures became more difficult, and several nearby flutter solutions were obtained clustered together, corresponding to different flutter modes. It then became apparent that a deeper insight into the fundamental nature of this eigenvalue problem could be achieved only if Eq. (10) were solved for the general eigenvalues B_R and B_I corresponding to given values of A_R and A_I. Accordingly, a master plot of the complex general eigenvalues B_R and B_I was obtained by evaluating $\Phi(B_R, B_I)$ for given values of A_R and A_I and finding what values of B_R and B_I made $\Phi(B_R, B_I) = 0$. From this master plot, the behavior and origin of all of the different eigenvalue branches for this continuous system could be seen. Then, using Eqs. (11a–11d), the pertinent physical parameters of this specific problem (μ, ϵ, Q, α, and β) could be solved in terms of the general eigenvalue parameters A_R, A_I, B_R, and B_I. Such solutions for physical eigenvalues of the type $\Omega = \alpha \pm i\beta$ are given in Appendix A. Special solutions for physical eigenvalues of the type $\Omega = \alpha$ and $\Omega = \pm i\beta$ are given also.

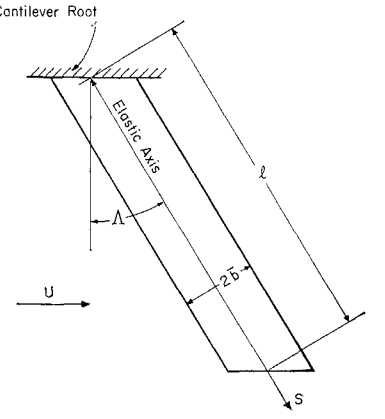

Fig. 1 Wing geometry and layout.

§ The function Φ, rather than the determinant Δ itself, is evaluated to prevent the possibility of repeated roots causing the determinant to approach zero. Also, the function Φ, unlike the determinant Δ, will preserve its sign if one replaces z_1 by z_2, etc.

The master plot of complex general eigenvalues B_R and B_I also can be used to solve other eigenvalue problems characterized by the general equation [Eq. (10)] and boundary conditions in Eq. (8) through reinterpretation of the coefficients A_R, A_I, B_R, and B_I. In Appendix B, solutions are given for the flutter speed, using the complete Theodorsen function $C(k) = F + iG$ and also with additional structural damping present in the system.

The procedure for solving Eqs. (4) and (8) through master plots of A_R, A_I, B_R, and B_I general eigenvalues displays great flexibility and can show much insight into the behavior and origin of instabilities for continuous systems, where many higher modes are present. It should be mentioned that Eq. (10) subject to boundary conditions in Eq. (8) has been studied already for the case $A_I = 0, B_I = 0$ by Movchan[7] in connection with the panel-flutter problem.

In conventional wing-flutter practice, it is often convenient to deal with a reduced velocity parameter, a reduced frequency k, and a frequency ratio ω/ω_h. It can be shown that

$$U(\cos\Lambda)F/\bar{b}\omega_h = 0.142(Q\mu/\epsilon)^{1/2} \tag{16}$$

$$k = \omega\bar{b}/U\cos\Lambda = 2F\beta(\epsilon/Q\mu)^{1/2} \tag{17}$$

$$\omega/\omega_h = (\beta/\omega_h)(EI/m\ell^4)^{1/2} = \beta/3.52 \tag{18}$$

The deflection shape $h(\xi, \tau)$ during a flutter condition is found from considering the real part of the right-hand side of Eq. (9). The complex function $\bar{h}(\xi) = \bar{h}_R + i\bar{h}_I$ is given by Eq. (12), where the roots z_m are those for the given flutter condition, and the complex constants c_m are to be found from Eq. (13). Setting $c_4 = 1$ and solving the first three equations of the matrix equation [Eq. (13)] for c_1, c_2, and c_3 will give

$$c_m = -N_m/D \qquad (m = 1, 2, 3) \tag{19}$$

where

$$c_4 = 1$$

$$D = \begin{vmatrix} 1 & 1 & 1 \\ z_1 & z_2 & z_3 \\ z_1^2 e^{z1} & z_2^2 e^{z2} & z_3^2 e^{z3} \end{vmatrix}$$

$$N_1 = \begin{vmatrix} 1 & 1 & 1 \\ z_4 & z_2 & z_3 \\ z_4^2 e^{z4} & z_2^2 e^{z2} & z_3^2 e^{z3} \end{vmatrix} \tag{20}$$

$$N_2, N_3 = \text{etc.}$$

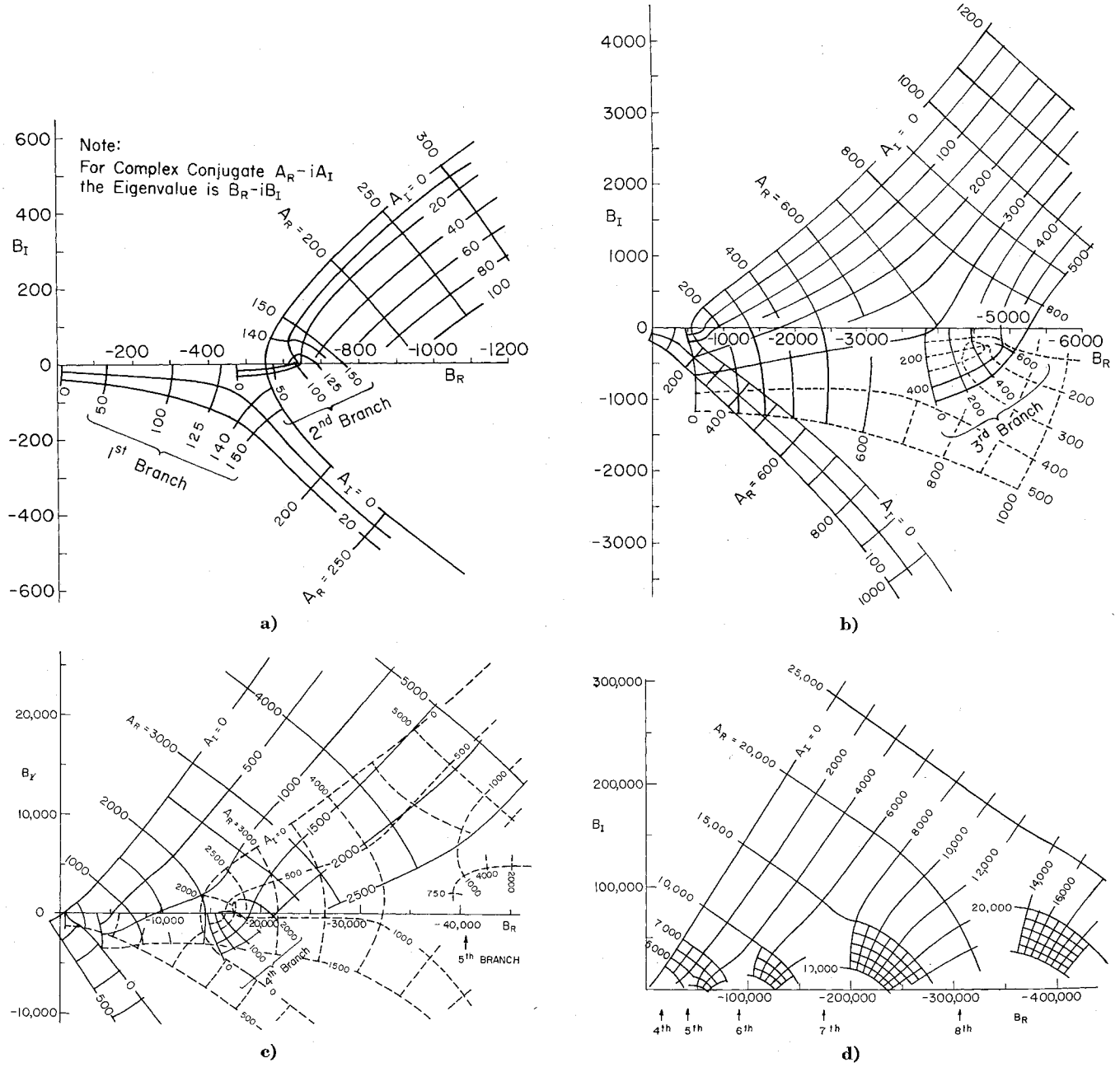

Fig. 2 Master plot of general eigenvalues.

Then, taking the real part of the right-hand side of Eq. (9), gives at flutter

$$h(\xi, \tau) = \bar{h}_R \cos\beta\tau - \bar{h}_I \sin\beta\tau \qquad (21)$$

This can be plotted for various times during one cycle ($\beta\tau = 2\pi$) to give a physical picture of the deflection shape during flutter.

2. Results and Discussion

Equations (10) and (8) were solved numerically at first by a General Precision LGP-30 computer and later by an IBM 1620 computer. Master plots of the general eigenvalues B_R and B_I corresponding to given values of A_R and A_I are given in Fig. 2. The origination and subsequent behavior of the first four branches is apparent. The origination of the fifth to eighth branches is also shown, but only the behavior of the most critical branches for this problem (highest positive B_I for a given positive A_R, A_I) are indicated. Note that the curves of constant A_R and A_I are always orthogonal and have the same scale interval. Only positive values of A_I are indicated since, for the complex conjugate $A_R - iA_I$, the eigenvalue is $B_R - iB_I$. This makes the curves continuous across the $A_I = 0$ boundaries when $B_I \neq 0$.

A plot of $A_R/-B_R$ vs A_R is given in Fig. 3 for the $A_I = 0$ and $B_I = 0$ general eigenvalues of Fig. 2. This was useful in obtaining eigenvalues of the form $\Omega = \alpha$, as described in Appendix A.

The below-flutter response of the swept wing with quasi-steady lift forces was obtained using Appendix A. Although not shown here, it is given in Ref. 9 and indicated the presence also of real, negative roots $\Omega = \alpha$ for certain speed ranges at low values of μ.

A plot of the flutter-speed parameter $U_F(\cos\Lambda)F/\bar{b}\omega_h$ vs μ is given in Fig. 4. The corresponding frequency at flutter β_F vs μ is given in Fig. 5. These were obtained from the master plots of the general eigenvalues using Appendix A. The scalloping at low values of μ and high ϵ results from the switching to higher, more critical, branches (modes). These plots show that the flutter speed increases sharply at low μ. Below certain critical values of μ, flutter does not occur. The reduced frequency k at flutter can be found from Figs. 4 and 5 using Eqs. (17) and (18). This k varies from zero at high μ to values greater than unity at low μ.

The deflection mode shapes $h(\xi, \tau)$ during a flutter condition are given in Fig. 6 for $\epsilon = 0.025$ and two values of μ. The mode shapes change from a standing wave-type at high values of μ to a traveling wave-type at low μ. It is apparent that a modal-type analysis would require the inclusion of many higher modes in order to approximate the deflection shape at low μ.

The preceding discussion and results for swept-wing flutter pertained to the use of quasi-steady lift forces, which resulted in Eq. (4). The swept wing can also be analyzed using the more complete unsteady lift forces with the Theodorsen function $C(k) = F + iG$. This analysis is given in Appendix B

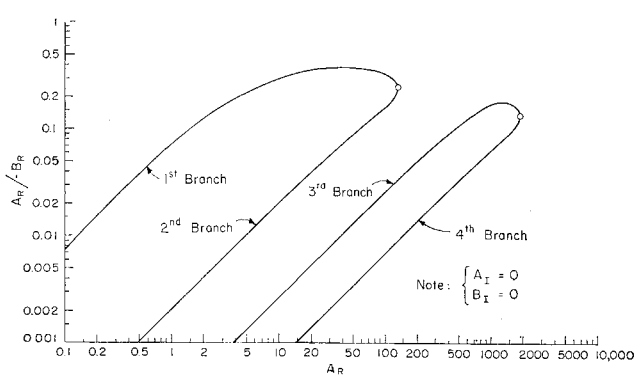

Fig. 3 Plot of real eigenvalues.

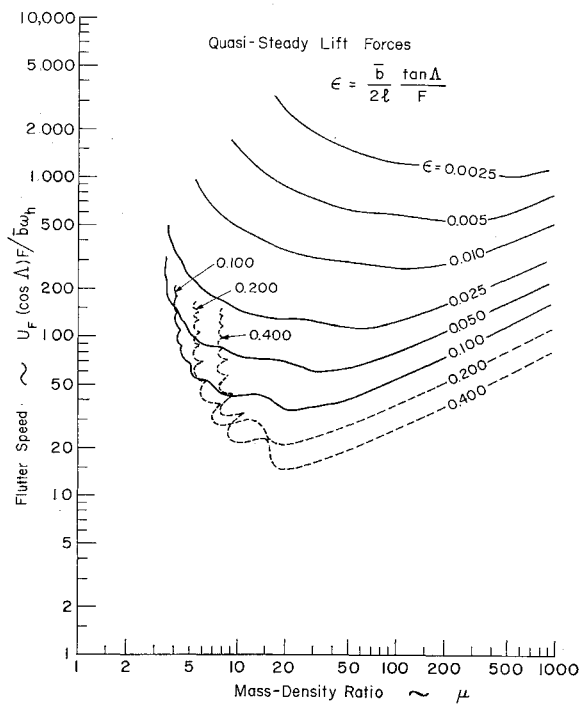

Fig. 4 Flutter speed vs μ (quasi-steady).

and uses the master plots of the general eigenvalues together with some additional data given in Fig. 7. The resulting flutter-speed parameter $U_F \cos\Lambda/\bar{b}\omega_h$ vs μ is given in Fig. 8, and the corresponding frequency at flutter β_F vs μ is given in Fig. 9. These plots again show the characteristic scalloping, the sharp rise in $U_F \cos\Lambda/\bar{b}\omega_h$ at low values of μ, and the critical values of μ below which flutter does not occur. In addition, new low flutter speeds are now present at high values of μ and ϵ involving flutter in the first branch (mode) as can be seen since $\beta_F \approx 4$. It is this new type of flutter that was investigated previously by Cunningham,[6] using modal methods, and was designated by him as single-degree-of-freedom flutter. The reduced frequency k at flutter again varies from zero at high μ to values greater than unity at low μ.

Figure 10 presents $U_F \cos\Lambda/\bar{b}\omega_h$ vs $\tilde{\epsilon}$ for various values of μ. At low values of μ, the flutter speed U_F decreases with increasing sweepback until a critical angle is reached beyond which the flutter speed rises sharply to infinity.

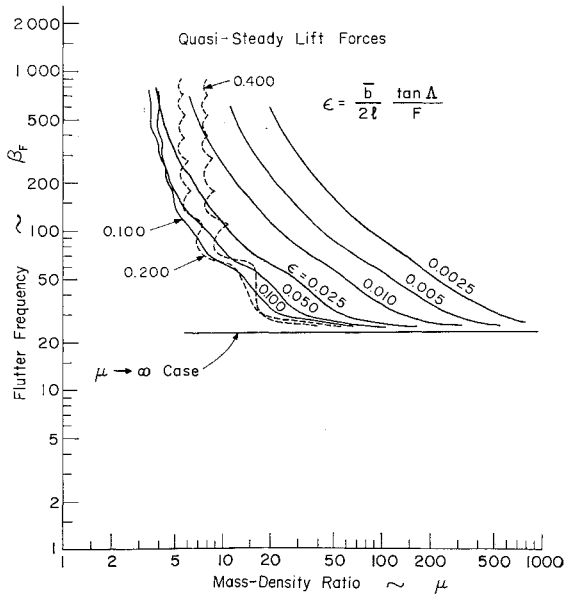

Fig. 5 Flutter frequency vs μ (quasi-steady).

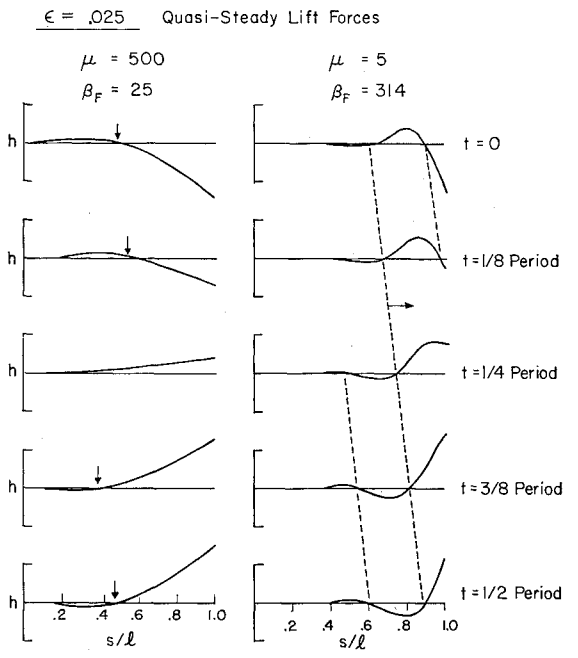

Fig. 6 Mode shapes at flutter (quasi-steady).

The deflection mode shapes at flutter are presented in Fig. 11. Again, the mode shapes change from a standing wave-type at high μ to a traveling wave-type at low μ. Also, more of the first-mode component is present in the $\mu = 500$ exact $C(k)$ case than was present in the $\mu = 500$ quasi-steady case. For higher $\tilde{\epsilon}$, the $\mu = 500$ exact $C(k)$ case would be almost a pure first-mode standing wave as surmised in Ref. 6.

A comparison of quasi-steady [$C(k) = 1$] and exact $C(k)$ flutter speeds is presented in Fig. 12. The quasi-steady case is seen to be generally unconservative in its estimate of the flutter speed except at high μ and low $\tilde{\epsilon}$ combinations, where it is in good agreement. Both theories indicate the sharp rise in flutter speed at low μ. However, the exact $C(k)$ lift forces also give rise to a new type of flutter at high μ and high $\tilde{\epsilon}$ combinations associated with low flutter speeds in predominantly the first mode (single-degree-of-freedom flutter). The results of Cunningham's single-degree-of-freedom modal analysis are also given. It seems that many more modes would be required in a modal analysis to extend down to the low μ range.

An investigation of the effects of additional structural damping was also made. Figure 13 shows the effect of adding a typical, small structural damping $g = 0.03$ on the exact

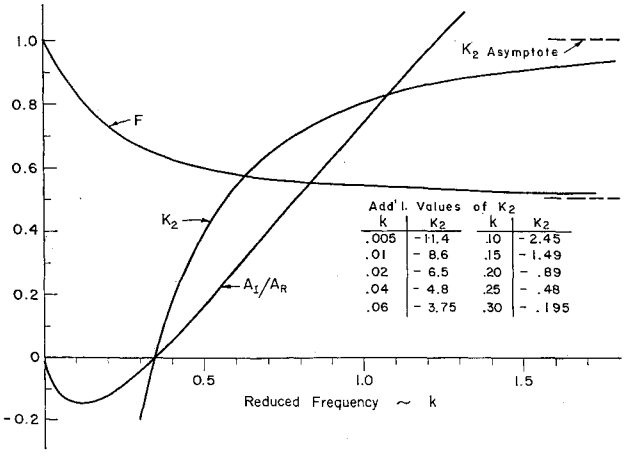

Fig. 7 Unsteady parameters vs k.

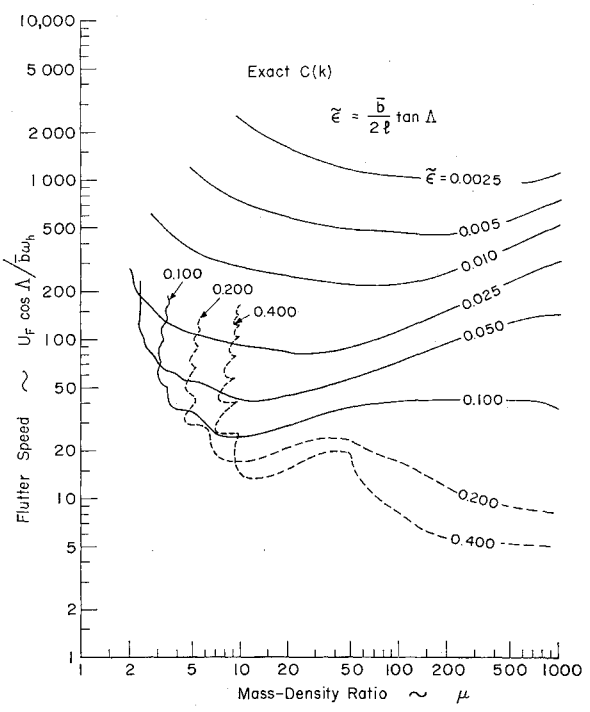

Fig. 8 Flutter speed vs μ [exact $C(k)$].

$C(k)$ flutter speeds. It has negligible effect except in the high μ, high $\tilde{\epsilon}$ range, where the flutter speed may be raised 2 or 3 times. This marked effect on the single-degree-of-freedom flutter speeds was also noted in Ref. 6.

For interest, the preceding pure bending flutter theory was applied to the uniform swept wing of Ref. 4 which was observed to have fluttered experimentally. For model 3 of that report, the pertinent nondimensional parameters are

$$\mu = 0.095 \qquad U_F \cos\Lambda/\omega_h \bar{b} = 5.20$$

$$\tilde{\epsilon} = 0.0156 \qquad \beta_F = 1.63$$

$$Q_F = 220 \qquad k = 0.088$$

The theory for these values of μ and $\tilde{\epsilon}$ would indicate that flutter was not possible. This disagrees with the observed results. It seems then that pure bending flutter is insufficient

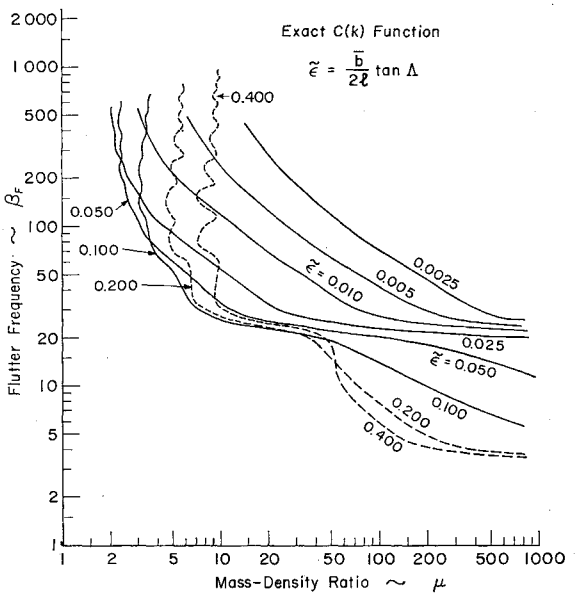

Fig. 9 Flutter frequency vs μ [exact $C(k)$].

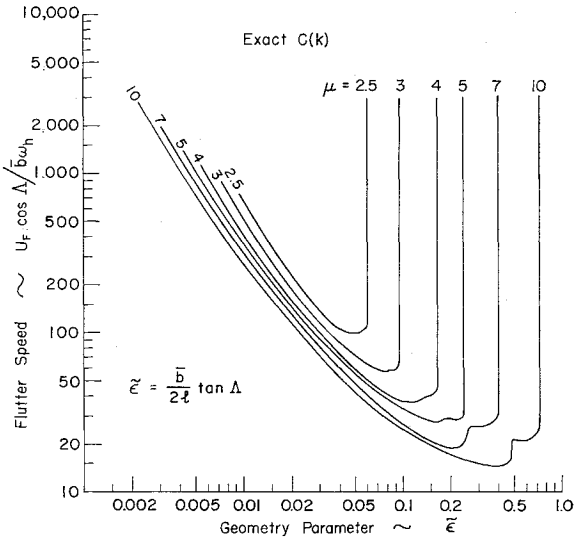

Fig. 10 Flutter speed vs $\tilde{\epsilon}$ at low values of μ [exact $C(k)$].

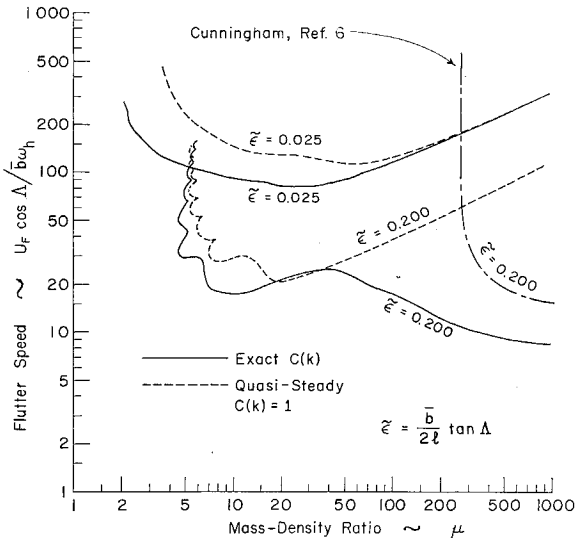

Fig. 12 Comparison of quasi-steady and exact $C(k)$ flutter speed.

to explain the particular flutter observed in Ref. 4. Probably the aspect ratio of the particular example is too low. A more elaborate theory involving torsion of the wing as well would have to be used there. Also the application of any aerodynamic-strip theory itself may be questionable,¶ in view of the strong spanwise gradients indicated by the wing mode shapes at low μ.

3. Conclusions

The pure bending flutter of a uniform, high-aspect ratio, swept wing has been studied in detail. An exact solution of the resulting nondimensional partial differential equation has revealed the nature of the eigenvalues and their behavior. The mathematical solution is similar to that used for panel-flutter problems[7, 8] and eliminates difficulties associated with convergence of modal solutions. The solution procedure may be used for other similar types of eigenvalue problems.

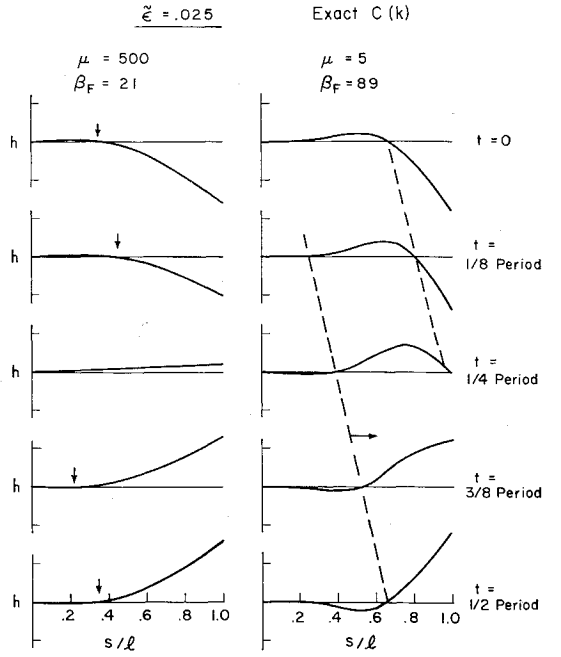

Fig. 11 Mode shapes at flutter [exact $C(k)$].

For the pure bending flutter of a swept wing, flutter does not occur below certain critical values of mass-density ratio μ. This behavior is also observed for bending-torsion flutter. Also, at the lower values of μ, increasing the sweepback of a given wing lowers the flutter speed significantly until a certain critical angle is reached beyond which the flutter speed rises sharply to infinity, and the wing becomes flutter-free.

The mode shapes at flutter were found to change from a standing wave-type flutter at high values of μ to a traveling wave-type at low μ. Modal-type analyses would require the use of many modes to represent the system at low values of μ.

Comparison of quasi-steady theory with the exact $C(k)$ revealed that quasi-steady theory is generally unconservative in its estimate of the flutter speed except at high μ and low $\tilde{\epsilon}$ combinations. Also, the exact $C(k)$ gives rise to a new type of flutter at high μ and high $\tilde{\epsilon}$ combinations, associated with flutter in predominantly the first bending mode, as first observed by Cunningham.[6] The addition of small structural damping has little effect on the flutter speed except for the first-mode flutter at high μ and high $\tilde{\epsilon}$ combinations.

The pure bending flutter theory does not explain the behavior of wing model 3 cited in Ref. 4, probably because the aspect ratio there is too low. To explain this and to understand more fully the effect of sweepback on low μ flutter, a

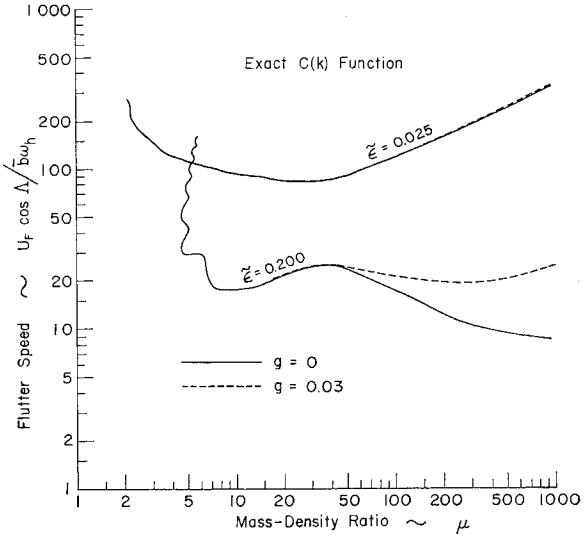

Fig. 13 Effect of structural damping.

¶ This was pointed out to the authors by the reviewer.

more elaborate theory involving the torsion of the wing as well should be developed in the manner of this report. Also, as mentioned previously, the aerodynamic-strip theory itself may have to be modified.

Appendix A: Physical Solution for Quasi-Steady Case

For quasi-steady lift forces, solutions for physical eigenvalues of the type $\Omega = \alpha \pm i\beta$ can be worked out from the eigenvalue master plot (Fig. 2). The relations between the general eigenvalues and the pertinent physical parameters of the flutter problem are given by Eqs. (11a–11d) of Sec. 1. The quantities A_R, A_I, B_R, B_I, and ϵ will be assumed given, and Eqs. (11a–11d) will be solved for the appropriate Q, μ, α, and β. From Eqs. (11a) and (11b), it is obtained that

$$\alpha = (\mu/\epsilon Q)^{1/2}(A_R - Q) \tag{A1}$$

$$\beta = (\mu/\epsilon Q)^{1/2}A_I \tag{A2}$$

Placing these into Eqs. (11c) and (11d) gives

$$\epsilon B_R = (A_R - Q) + [(A_R - Q)^2 - A_I^2](\mu + 1)/Q \tag{A3}$$

$$\epsilon B_I = A_I + 2(A_R - Q)A_I(\mu + 1)/Q \tag{A4}$$

Solving Eq. (A4) for $(\mu + 1)/Q$ and placing this into Eq. (A3) results in a quadratic equation in $(A_R - Q)$ which can be solved to give

$$(A_R - Q) = \frac{\epsilon B_R}{2(1+p)} \pm \left[\left(\frac{\epsilon B_R}{2(1+p)}\right)^2 + \frac{pA_I^2}{1+p}\right]^{1/2} \tag{A5}$$

where

$$p = \tfrac{1}{2}[(\epsilon B_I/A_I) - 1] \tag{A6}$$

The quantities Q and μ are then found from the equations

$$Q = A_R - (A_R - Q) \tag{A7}$$

$$\mu = [Qp/(A_R - Q)] - 1 \tag{A8}$$

and the quantities α and β are found from Eqs. (A1) and (A2). For a given ϵ, any combination of A_R, A_I, B_R, and B_I from Fig. 2 which gives real, positive values of Q and μ represents a solution of the type $\Omega = \alpha \pm i\beta$.

Special solutions for physical eigenvalues of the type $\Omega = \alpha$ may also be worked out. These correspond to aperiodic responses. In Eqs. (11a–11d) let $\beta = 0$. Equations (11b) and 11d) then yield the requirement $A_I = 0$ and $B_I = 0$. Equation (11a) can be solved for α to give Eq. (A1). Placing this into Eq. (11c) and solving the resulting quadratic equation for Q gives

$$Q = \left[\left(\frac{1+2\mu}{2\mu}\right)A_R + \frac{\epsilon B_R}{2\mu}\right] \pm \left\{\left[\left(\frac{1+2\mu}{2\mu}\right)A_R + \frac{\epsilon B_R}{2\mu}\right]^2 - \left(\frac{\mu+1}{\mu}\right)A_R^2\right\}^{1/2} \tag{A9}$$

The corresponding value of α is obtained from Eq. (A1). For given μ and ϵ, any combination of A_R, B_R, $A_I = 0$, and $B_I = 0$ from Fig. 3 which gives real, positive values for Q in Eq. (A9) represents a solution of the type $\Omega = \alpha$. It can be shown further that real, positive values of Q will occur in Eq. (A9) only if

$$A_R/-B_R > \epsilon\{1 + 2\mu + 2[\mu(\mu+1)]^{1/2}\} \tag{A10}$$

Special solutions for physical eigenvalues of the type $\Omega = \pm i\beta$ may also be worked out. These correspond to flutter points. In Eqs. (11a–11d), let $\alpha = 0$. This results in the requirement

$$Q = A_R \tag{A11}$$

Combining the remaining equations gives

$$\epsilon = A_I/B_I \tag{A12}$$

$$\beta = \pm[\mu/(\mu+1)]^{1/2}(-B_R)^{1/2} \tag{A13}$$

$$\mu = -B_R(A_R/B_IA_I) - 1 \tag{A14}$$

Any combination of A_R, A_I, B_R, and B_I from Fig. 2 which gives real, positive values for Q, μ, ϵ, and β represents a solution of the type $\Omega = \pm i\beta$.

Appendix B: Flutter Solution with Exact $C(k)$ and Structural Damping

For unsteady lift forces involving the exact $C(k) = F + iG$ and for additional structural damping present, flutter solutions of the type $\Omega = \pm i\beta$ can be worked out from the eigenvalue master plot (Fig. 2). The basic beam differential equation is now

$$EI(\partial^4 h/\partial s^4) = \tilde{L} - m(\partial^2 h/\partial t^2) - D_B(\partial h/\partial t) \tag{B1}$$

where $\tilde{L}$ is given by Eq. (2), and the assumed constant damping D_B can be expressed as

$$D_B = g_h m\omega_h \tag{B2}$$

The form of Eq. (B2) implies that the structural damping coefficient g_j of the higher modes ω_j will be given by $g_j = g_h\omega_h/\omega_j$. For metal wings, g_h ranges from 0 to 0.03 approximately.

Introducing nondimensional variables ξ and τ into Eq. (B1), setting

$$h(\xi, \tau) = \bar{h}(\xi)e^{i\beta\tau} \tag{B3}$$

and nondimensionalizing, as before, will now result in the differential equation

$$(d^4\bar{h}/d\xi^4) + \{Q + i[\beta(Q\epsilon/\mu)^{1/2} + QG/F]\}(d\bar{h}/d\xi) + \{-[(\mu+1)\beta^2/\mu + (G\beta/F)(Q/\mu\epsilon)^{1/2}] + i[\beta(Q/\mu\epsilon)^{1/2} + 3.52g_h\beta]\}\bar{h} = 0 \tag{B4}$$

For the exact $C(k)$ case, it is better to define new parameters $\tilde{\epsilon}$ and $\tilde{Q}$ independent of F. Thus

$$\tilde{\epsilon} = \epsilon F = (\bar{b}/2\ell)\tan\Lambda \tag{B5}$$

$$\tilde{Q} = Q/F = \pi\rho U^2\bar{b}l^3(\sin 2\Lambda)/EI \tag{B6}$$

Introducing these parameters, and noting that the reduced frequency k is given by

$$k = \omega\bar{b}/U\cos\Lambda = 2\beta(\tilde{\epsilon}/\tilde{Q}\mu)^{1/2} \tag{B7}$$

the differential equation (B4) can be written in the basic form of Eq. (10), where the coefficients are now

$$A_R = \tilde{Q}F \tag{B8}$$

$$A_I = K_2\beta(\tilde{Q}\tilde{\epsilon}/\mu)^{1/2} \tag{B9}$$

$$B_R = -[(\mu + K_2)/\mu]\beta^2 \tag{B10}$$

$$B_I = \beta F(\tilde{Q}/\mu\tilde{\epsilon})^{1/2} + 3.52g_h\beta \tag{B11}$$

and the factor K_2 is a function of k defined by

$$K_2 = 1 + 2G/k \tag{B12}$$

As before, these equations can be solved for $\tilde{Q}$, $\tilde{\epsilon}$, μ, β, and k in terms of A_R, A_I, B_R, B_I, and g_h.

First, using Eqs. (B9, B11, and B10) gives

$$\tilde{\epsilon} = FA_I/K_2(B_I - 3.52g_h\beta) \tag{B13}$$

$$\beta = [\mu/(\mu + K_2)]^{1/2}(-B_R)^{1/2} \tag{B14}$$

Then, from Eqs. (B13, B9, B14, and B8), after much

algebra, it is obtained that the

$$\mu = K_2(R - 1) + [K_2H/(1 - H^2)]\{H(R - \tfrac{1}{2}) \pm [R(R - 1) + (H^2/4)]^{1/2}\} \quad \text{(B15)}$$

where

$$R = -B_RA_R/B_IA_I \quad \text{(B16)}$$

$$H = 3.52g_h(-B_R)^{1/2}/|B_I| \quad \text{(B17)}$$

and the + or − sign is chosen such as to make the whole second term on the right-hand side of Eq. (B15) a positive quantity. Then, using Eqs. (B13, B14, and B17), it is obtained that

$$\tilde{\epsilon} = FA_I/K_2B_I\{1 - H[\mu/(\mu + K_2)]^{1/2}\} \quad \text{(B18)}$$

Finally, it is noted that

$$kK_2/2F = A_I/A_R \quad \text{(B19)}$$

Equation (B19) relates implicitly the value of k to A_I and A_R.

Equations (B19, B12, B15, B18, B14, and B8) permit one to convert points on the master plot into values of k, μ, $\tilde{\epsilon}$, β, and $\tilde{Q}$. For convenience, Fig. 7 shows plots of F, K_2, and A_I/A_R vs k. Any combination of A_R, A_I, B_R, and B_I which gives real, positive values for μ, $\tilde{\epsilon}$, $\tilde{Q}$, and β represents a flutter point. Note that, in the unsteady case, K_2 may be negative. From Eq. (B18), this permits some physical solutions for A_I and B_I of opposite sign, unlike the quasi-steady case. It is this new region that gives rise to the single-degree-of-freedom flutter noticed by Cunningham.[6]

References

[1] Theodorsen, T. and Garrick, I. E., "Mechanism of flutter, a heoretical and experimental investigation of the flutter problem," Langley Memorial Aeronautical Lab. NACA TR 685 (1940).

[2] Henry, C. J., Dugundji, J., and Ashley, H., "Aeroelastic stability of lifting surfaces in high density fluids," J. Ship Res. **2**, 10–21 (March 1959).

[3] Herr, R. W., "A study of flutter at low mass ratios with possible application to hydrofoils," NASA TN D-831 (1961).

[4] Baird, E. F., Squires, C. E., Jr., and Caporali, R. L., "An experimental and theoretical investigation of hydrofoil flutter," Aerospace Eng. **21**, 34–41 (February 1962).

[5] Caporali, R. L. and Brunelle, E. J., "Hydrofoil instability at low mass density ratios," Aerospace and Mechanical Sciences Rept. 670, Princeton Univ. (March 1964).

[6] Cunningham, H. J., "Analysis of pure-bending flutter of a cantilever swept wing and its relation to bending-torsion flutter," Langley Aeronautical Lab. NACA TN 2461 (1951).

[7] Movchan, A. A., "On vibrations of a plate moving in a gas," NASA Republ. 11-22-58 W (January 1959); transl. from Prikl. Mat. Mekh. **20**, no. 20, 211–222 (1956).

[8] Hedgepeth, J. M., "Flutter of rectangular simply supported panels at high supersonic speeds," J. Aeronaut. Sci. **24**, 563–573 (1957).

[9] Dugundji, J. and Ghareeb, N., "Pure bending flutter of a swept wing in a high density, low speed flow," Fluid Dynamics Research Group Rept. 64-1, Massachusetts Institute of Technology (March 1964).

[10] Bisplinghoff, R. L., Ashley, H., and Halfman, R. L., *Aeroelasticity* (Addison-Wesley Publishing Co., Inc., Cambridge, Mass., 1955), 1st ed., Chap. VII, p. 398, Eq. (7-69).

[11] Dugundji, J., "Effect of quasi-steady air forces on incompressible bending-torsion flutter," J. Aeronaut. Sci. **25**, 119–121 (1958).

[12] Gravitz, S. I., Laidlaw, W. R., Bryce, W. W., and Cooper, R. E., "Development of a quasi-steady approach to flutter and correlation with kernel-function results," J. Aerospace Sci. **29**, 445–459 (1962).